

Chapter 4:
Biophysical studies of L1-mediated homophilic adhesion

Introduction

L1 is a transmembrane glycoprotein that mediates homophilic and heterophilic adhesion events in neural cell recognition (1). L1 is an immunoglobulin superfamily member composed of six Ig-like domains followed by five fibronectin type III (FNIII) domains, a transmembrane domain and a short but well-conserved intracellular domain (2). L1 interacts with various binding partners and plays important roles in neural development as well as in the adult nervous system, including neurite outgrowth, neuronal migration and survival, and synapse organization (3, 4). Mutants of L1 have been found to cause mental retardation, hydrocephalus, impairment of sensorimotor gating, abnormal cerebellar development, and many other phenotypes (5-8).

Studies have shown that the first four Ig domains of L1 form a horseshoe shaped structure, which has been reported to be critical in L1 homophilic adhesion (9, 10). Based on studies of its homologues, two models, the domain-swapped multimer model (9) and the zipper model (11), have been proposed to explain how homophilic interaction is achieved. In the domain-swapping model, transient opening of the horseshoe structure induces the formation of domain swapped dimers and multimers (Figure 4A), and the latter contains periodic adhesion sites with gaps in between. The zipper model, however, predicts a continuous linear array of horseshoes in the middle of the adjacent membranes (Figure 4B). The two models not only differ in the adhesion site pattern, but also in the inter-membrane distance. Dr. Yongning He, a postdoctoral scholar in the Bjorkman laboratory, initiated his electron microscopy studies to observe L1-mediated adhesion between liposomes and to verify or refute these models. His studies revealed a regularly spaced pattern formed by L1 molecules from neighboring membranes and found that

alterations of L1-associated carbohydrates, for example, recombinant L1 proteins from different expression systems, changed the adhesion interface, particularly the distance of adhesion sites. Based on all of these observations, he suggested a carbohydrate-modified interaction model, in which protein-protein interactions determine the *trans* interaction by pairs of horseshoe domains and carbohydrate-carbohydrate or carbohydrate-protein interactions regulate the *cis* spacing between neighboring L1 proteins on a membrane (12) (Figure 4C).

Additional questions regarding L1-mediated adhesion remain to be addressed. For example, what is the average binding strength between one pair of molecules (or average energies at different molecular densities)? Is there cooperativity in adhesive interactions between membranes? That is, is the total adhesion energy at an interface with 100 molecules exactly twice of that of an interface with 50 molecules? Additionally, under physiological conditions, when L1 protein is present at relatively low densities, does an adhesion interface recruit molecules from other regions?

In order to address these questions, an appropriate model system is needed. Studies of membrane mechanics within the context of biology has long been a field that attracts physicists. Artificial lipid vesicles are often used as a model system for studying membrane mechanics because unlike biological membranes in cells, their lack of a cytoskeleton matrix and various membrane proteins makes it easier for researchers to understand underlying physical mechanisms and to provide important insights into complex biomembranes (13). Experimental and theoretical/numerical approaches have been applied to the study of red blood cell shape determination and transition (14),

budding (exocytosis) (15), and adhesion (16, 17). For a review of this field, please refer to (13).

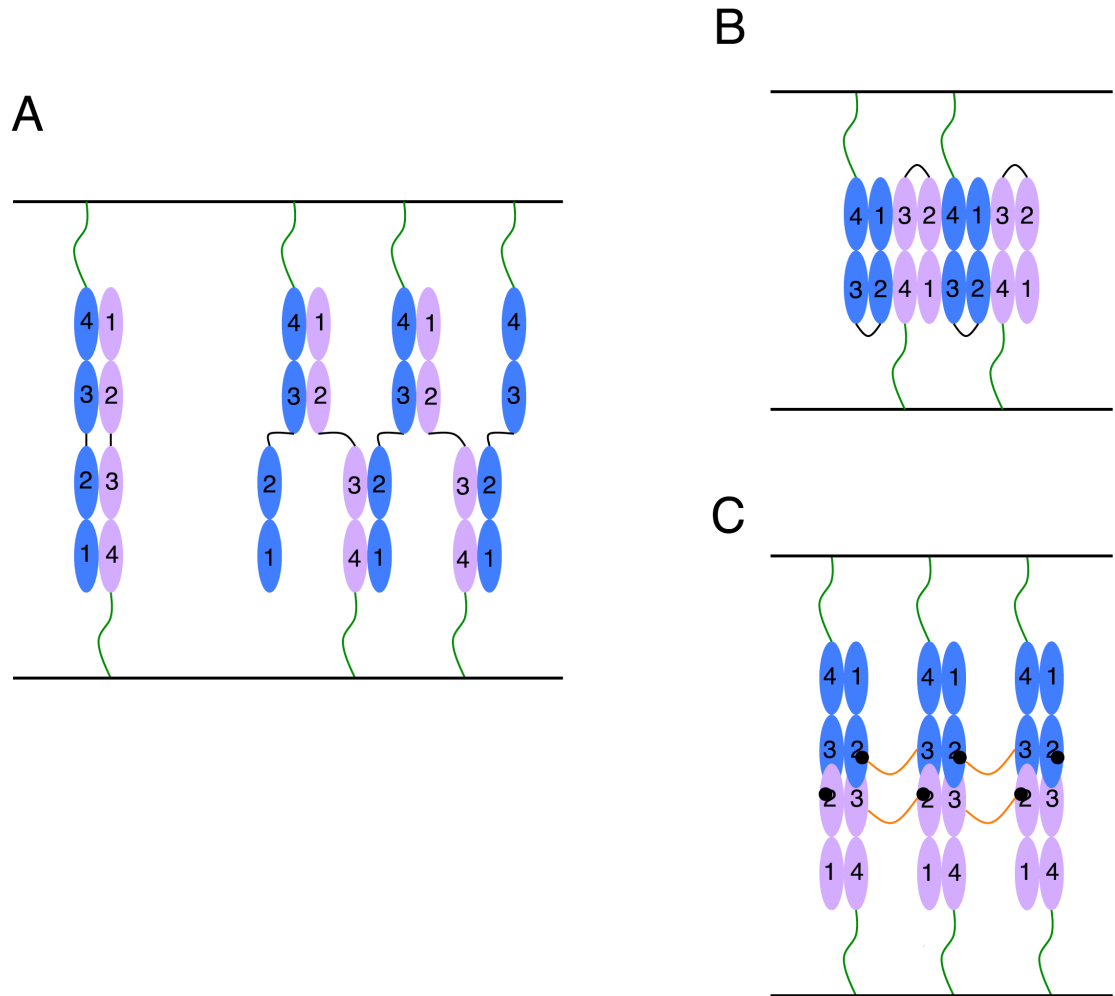


Figure 1. Three models of L1-mediated homophilic adhesion. (A) Domain-swapping model suggested by the structure of hemolin, an L1 homologue (9). (B) Zipper model based on the packing in crystals of axonin-1, another L1 homologue (11). (C) Carbohydrate-modified model proposed on the basis of electron tomography studies of L1-mediated adhesion in liposomes (12). Negatively-charged sialic acids on carbohydrates from one horseshoe interact with a positive patch (represented by a black dot) of a neighboring horseshoe to form a regularly spaced pattern. (Figure modified from (12).)

Our studies of L1-mediated adhesion have been a collaborative effort with Tristan Ursell, a former graduate student in the Phillips laboratory and now a postdoctoral scholar at Stanford. We aim to use biophysical approaches to answer the questions listed above using giant unilamellar vesicles (GUVs) as a platform. Tristan and I independently developed a basis shape model for the deformation for a GUV adhered to a flat substrate. In this general model, adhesion strength is defined on the interface but the nature of the adhesion force is not specified – it can be any interaction. Simulations were performed to show how adhesion energy density affects the shape of an adhered GUV. Experimentally, we developed a complete protocol in order to image L1-coated GUV adhering to L1-functionalized coverglass using confocal microscopy. Data processing scripts were written in order to reconstruct three dimensional shape configurations and adhesion energy density was derived from the shape profile. We also tested the applicability of a numerical simulation program, Surface Evolver, to calculate the shape of a vesicle adhering to a substrate. Although the numerical method is not amenable to the inverse problem of extracting model parameters, it did provide insight regarding the validity of our parameterized basis shape model; by fitting the simulated profile to our model, it was possible to map out the regime where the latter indeed serves as a faithful characterization of the full profile.

Materials and Methods

Molecular cloning and protein expression

A gene encoding the ectodomain of human L1 (residues M1-E1120 and a C-terminal 6x-His tag) was cloned into pcDNA3.1 vector (Invitrogen) by Yongning He as

described in (12). Supernatants collected from transiently-transfected 293T cells were buffer exchanged into 20 mM Tris, pH 7.4, 150mM NaCl before loading onto a Ni-NTA column (Qiagen). Eluates were further purified by size exclusion chromatography using a Superdex 200 10/30 column (GE Healthcare). Proteins were concentrated and stored at 4 °C in 20 mM Tris pH 7.4, 150 mM NaCl and 5 mM EDTA.

Preparation of giant unilamellar vesicles

1,2-Dioleoyl-sn-Glycero-3-phosphocholine (DOPC), 1,2-Dioleoyl-sn-Glycero-3- $\{[N(5\text{-Amino-1-Carboxypentyl})\text{iminodiAcetic Acid}]\text{Succinyl}\}$ (nickel salt) (DOGS-NTA-Ni), and 1,2-Dioleoyl-sn-Glycero-3-Phosphoethanolamine-N-(Lissamine Rhodamine B Sulfonyl) (Rhodmaine-PE) were purchased from Avanti Polar Lipids (Alabaster, AL). Lipid mixtures were made by mixing 5 mole % DOGS-NTA-Ni with 94.5 mole % DOPC and 0.5 mole % Rhodamine-PE to facilitate visualization. The final concentration of lipids was set to 2 mg/ml in chloroform. 2 μl lipid/chloroform solution was applied to pre-cleaned indium tin oxide (ITO) glass slide on a custom-made chamber (by Tristan Ursell) to form a thin layer. The chamber was desiccated for one hour before an ethanol-cleaned one-side-greased nitrile O-ring was carefully placed on top of the dried lipid layer. 140 μl of 220 mM sucrose solution was added in the O-ring on which the cover of the chamber was then placed. Applying 1-5V voltage at 10 Hz to the chamber for 3 hours destabilized the lipid film to form GUVs. The end product was removed from the chamber and transfer to an eppendorf tube. The quality and yield of GUVs was checked under a microscope before proceeding to the next step.

Attaching protein to GUVs and collecting confocal images

Protein samples were exchanged into buffer containing 20mM Tris, 100mM NaCl before use (EDTA in the storage buffer needed to be removed to ensure that the His-tagged protein bound efficiently to the Ni-NTA head groups). Copper NTA functionalized glass cover-slips were obtained from MicroSurfaces, Inc. The GUV stock was diluted by 10 fold in 20mM Tris, 100mM NaCl. Wildtype L1 (or a negative control His-tagged protein, scFv b12, courtesy of Rachel Galimidi) was incubated separately with the functionalized glass cover-slip and the diluted GUVs for 40 minutes in order to attach the His-tagged protein on both surfaces through His-tag metal-NTA chelation. L1-decorated GUVs were then incubated with the glass coverslips to allow the adhesion of GUVs onto the bottom of the coverslip. After 20 minutes of incubation, samples were placed on the stage of Perkin-Elmer Ultraview spinning disk microscope and confocal images were recorded using a 100X oil-immersed objective (α Plan-APOCHROMAT 1.46 Oil DIC, Zeiss) with 568nm laser as the excitation source. 3-D confocal stacks were sampled at 0.2 μ m spacing in z direction with 200 milliseconds exposure time for each image.

Data analysis with Matlab

The following steps summarize how to extract an adhesion energy from z-stack images of a vesicle adhering to a flat surface.

- (1) Format conversion

The confocal z-stack images had to be converted to TIFF using ImageJ PerkinElmer plugin in batch model. These images correspond to a series of optical sections covering the whole vesicle.

(2) Determination of axis of revolution

The images from the equatorial region of the vesicle normally have the best image quality in terms of signal to background ratio. It is thus possible to choose a threshold to convert the grayscale image to binary format, which displays background as black and the lipid bilayer as white. A circle could be fit using those points corresponding to the bilayer. Due to the high signal to background ratio, the exact choice of the threshold value did not have a significant impact on the fitting result. Ten images from the equatorial region were analyzed this way, and the coordinates of the center of the fitted circles were averaged to give the position of the revolution axis of the vesicle.

(3) Determination of shape profile

For images far from the equatorial region, it was difficult to find a threshold to differentiate bilayer and background; the vesicle boundary appeared to be a thick circle. In order to increase the signal to background ratio, a self-averaging approach, based on the axisymmetric property of the vesicle, was employed. To be specific, the image was divided into a series of concentric circular shells around the axis of revolution determined in the previous step. The average grayscale value in each shell was calculated and plotted as a function of its radial distance from the center. The peak of this radial profile indicated the position of vesicle boundary for this z-section.

(4) Determination of the geometric parameters

For each radial profile, a threshold was chosen as the maximum intensity minus the background. Points above that threshold had radial coordinates approximately the same as the radius of the vesicle at the z -section. Note that the z positions were corrected as described in detail in the next section (*Refractive index mismatch correction*). These experimentally determined vesicle profile points were used to determine the geometric parameters characterizing the vesicle shape. In particular, the theoretical profile of the vesicle is completely determined by three important parameters, namely, R_3 , λ , and θ_c (for details of the model, see Figure 2). Given the experimental profile, a three-parameter search was carried out to find a set of parameters that minimized the square difference between the theoretical and the experimental points. Due to the existence of local minima, many random points in the three-dimensional parameter space were chosen as starting points of the optimization process. The theoretical curve based on the optimized parameters was checked visually against the experimental data as shown in the lower left corner of Figure 2.

(5) Determination of adhesion energy

In the adhesion model, the three geometric parameters are obtained by minimizing the system free energy given the adhesion energy, bilayer bending modulus, vesicle area and reduced volume. It is thus possible for us to deduce the adhesion energy using the parameters obtained in step 4. Furthermore, the vesicle area and reduced volume are fixed by a given set of shape parameters (R_3 , λ , and θ_c) when the bilayer bending modulus for the DOPC lipid (the major component in our lipid mixture) is known. So the problem reduces to a one-dimensional search in the space of adhesion energy to

get the best agreement between geometric parameters determined from experiments and theory.

Refractive index mismatch correction

In order to reconstruct the three-dimensional shape of an adhered vesicles, the exact position along the z-axis is indispensable. Due to the difference of refractive indices between the cover-slip/immersion oil ($n=1.52$) and the imaging medium (here 20 mM Tris, pH 7.4, 100 mM NaCl, with $n=1.34$ (18)), the actual position of the focal plane differs from its nominal position since the direction of light changes as it enters the second medium from the first one. This effect worsens as the distance from the objective increases. For a thin specimen (less than 3 μm) or only minor differences in refractive indices between immersion and imaging media (for example, $n_1=1.46$, $n_2=1.52$), a linear correction factor can be used to account for the effects resulting from refractive index mismatch (19). In our case, the GUVs ranged from a few microns to tens of microns. Therefore, single parameter correction method was not appropriate. For every single confocal image, the position of actual focal plane was calculated based on a theory developed by Egner and Hell (20). The Matlab script for the correction is included in Appendix C.

Simulation using Surface Evolver

The initial shape is a cube on a flat surface and the bottom of the cube is confined to be on the surface. The vertices, edges, faces and body are defined, and the evolution of the vesicle shape is controlled by two energies: adhesion energy and bending energy. The

total area and total volume are fixed during evolution. The surface is first coarsely triangulated during the initial steps of evolution. After the shape starts to stabilize, the surface triangularization is refined to get finer details of the shape. The evolution sequence is normally composed of steps of first-order gradient search, facet management, refinement, and second-order Hessian search. The first-order gradient algorithm is robust but slow, so it is used to get close to the equilibrium point and provide a good starting point for second-order Hessian search. Facet management is required to get rid of extremely small edges and adjust the facet sizes to make them more uniform; robust calculation of curvature relies on this procedure. The grid density is adjusted by refinement to achieve the desired spatial resolution.

Results and Discussions

Parameterized basis shape model

As summarized in a classic review published in 1997 (13), there are three approaches that are often used to find the vesicle shape with the lowest energy: solving Euler-Lagrange equations, applying variational method to trial shapes, and minimizing the energy numerically on triangulated surfaces. We chose the second approach due to its relative simplicity, both analytically and numerically. The first method was attempted while I tried to repeat the results by Seifert in the two-dimensional adhering vesicle case (17) but the extension to three dimensions is nontrivial. The third strategy was later used to verify the validity of the current approach and will be described in later paragraphs.

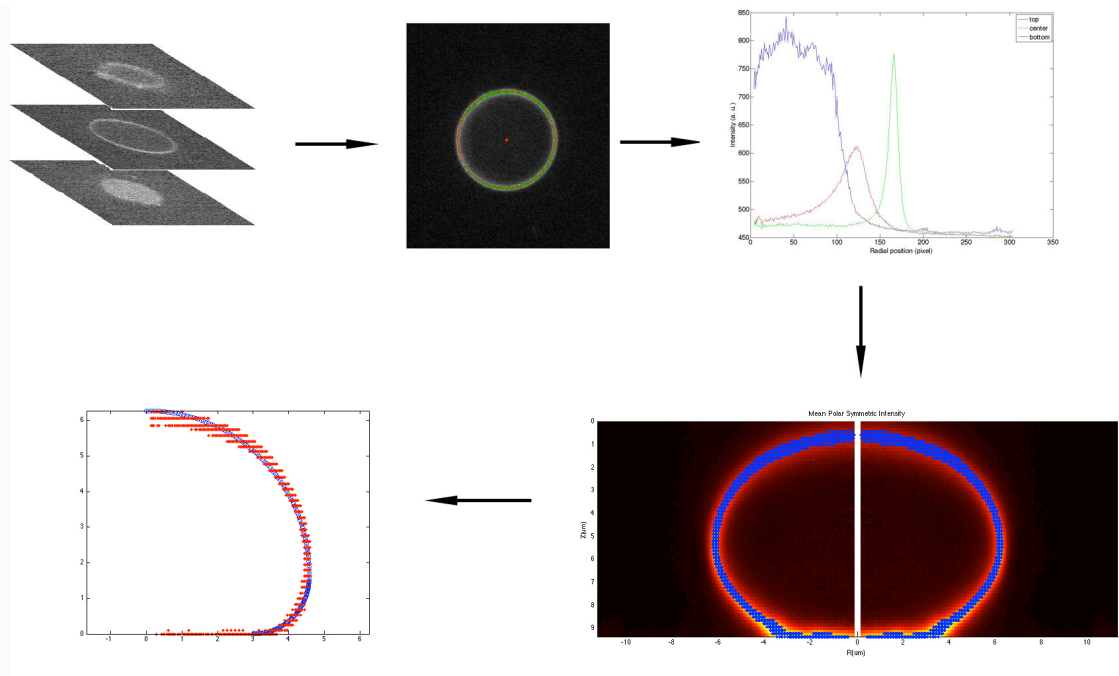


Figure 2. Flow chart showing how the confocal images were processed. Clockwise from top left: stacks of raw images, fitting equatorial data to find the revolution axis, plotting self-averaging intensity profile, extracting data points (blue) from background, fitting the data points to a 3-parameter shape profile.

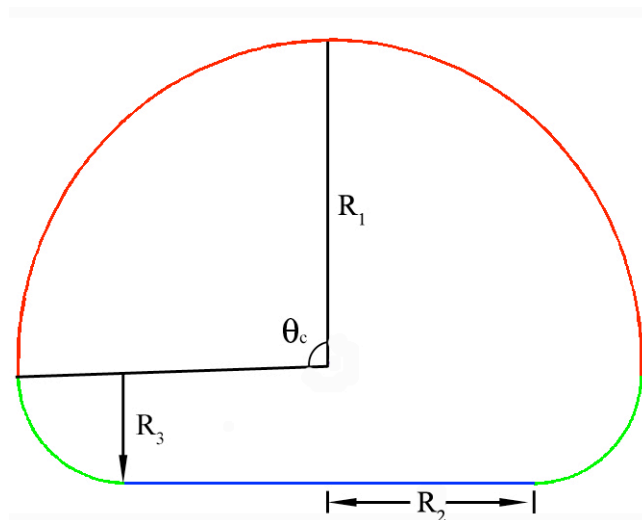


Figure 3. Schematic view of a vesicle adhering to a flat surface with the geometric parameters defined.

For simplicity, we consider a vesicle adhering to a flat surface. Due to the axisymmetric nature of the problem, one can use a cross section along the revolution axis to represent the 3-D object. Assume the initial state is a free GUV with total volume V_0 and total area A_0 ($A_0=4\pi R_0^2$, where R_0 is called characteristic length) and the final state is pictured below in Figure 3, parameterized by three radii R_1 , R_2 , R_3 and one angle θ_c . An adhered vesicle can be characterized by three regions: a spherical cap (in red), a adhering base (blue), and the connecting segment (green). Due to the boundary conditions, one radius can be expressed in terms of the other three parameters, leaving only three independent variables to fully describe the system. Let $\cos\theta_c=c$, and introduce $\lambda=R_2/R_3$, then we have

$$\begin{aligned} R_2 &= \lambda R_3 \\ R_1 &= R_3 \left(\frac{\lambda}{\sqrt{1-c^2}} + 1 \right) \end{aligned}$$

Now the system can be completely described by R_3 , λ , and c . The total area and total volume can be expressed as

$$\begin{aligned} A &= A_{ba} + A_{sc} + A_{co} \\ &= \pi R_2^2 + 2\pi R_1^2(1-c) + 2\pi R_3 [R_2 \arccos(-c) + R_3(1+c)] \\ &= \pi R_3^2 \left[\lambda^2 + \frac{2(\lambda + \sqrt{1-c^2})^2}{1+c} + 2\lambda \arccos(-c) + 2(1+c) \right], \end{aligned}$$

$$\begin{aligned} V &= \frac{2}{3}\pi R_3^3 \left(\frac{\lambda}{\sqrt{1-c^2}} + 1 \right)^3 (1-c) + \frac{\pi}{3} R_3^3 (\lambda + \sqrt{1-c^2})^2 \left(\frac{\lambda}{\sqrt{1-c^2}} + 1 \right) (-c) \\ &\quad + \pi \times \left[(1+c)\lambda^2 R_3^3 + c\sqrt{1-c^2}\lambda R_3^3 + (1+c)^2 R_3^3 - \frac{1}{3}(1+c)^3 R_3^3 + 2\lambda R_3^3 \arcsin \sqrt{\frac{1+c}{2}} \right]. \end{aligned}$$

The bending energy can be calculated as a summation of the contributions from the spherical cap and the connecting region

$$\begin{aligned}
E_{bending} &= E_{bending}^{sc} + E_{bending}^{co} \\
&= \frac{\kappa}{2} \int_0^{2\pi} d\phi \int_0^{\theta_c} \left(\frac{2}{R_1}\right)^2 R_1^2 \sin \theta d\theta + \frac{\kappa}{2} \int_0^{2\pi} d\phi \int_{\theta_c}^{\pi} (K_1 + K_2)^2 R_3 (R_2 + R_3 \sin \theta) d\theta \\
&= 4\pi\kappa(1-c) + \kappa\pi \int_{\theta_c}^{\pi} \left(\frac{1}{R_3} + \frac{\sin \theta}{R_2 + R_3 \sin \theta}\right)^2 R_3 (R_2 + R_3 \sin \theta) d\theta \\
&= 4\pi\kappa(1-c) + \kappa\pi \int_{\theta_c}^{\pi} \frac{(R_2 + 2R_3 \sin \theta)^2}{R_3(R_2 + R_3 \sin \theta)} d\theta
\end{aligned}$$

where K_1 and K_2 are the principal curvatures of the local surface. By definition, $R_2 = \lambda R_3$,

the bending energy becomes

$$E = 4\pi\kappa(1-c) + \kappa\pi \int_{\theta_1}^{\pi} \frac{(\lambda + 2 \sin \theta)^2}{(\lambda + \sin \theta)} d\theta$$

Depending the value of λ , the above integral has analytical form as following:

$$\begin{aligned}
\lambda > 1, I &= 4(1+c) + \frac{\lambda^2}{\sqrt{\lambda^2-1}} \left(\pi - 2 \arctan \left(\frac{1 + \lambda \sqrt{(1-c)/(1+c)}}{\sqrt{\lambda^2-1}} \right) \right) \\
\lambda = 1, I &= 4(1+c) + \frac{2}{1 + \sqrt{\frac{1-c}{1+c}}} \\
\lambda < 1, I &= 4(1+c) + \frac{\lambda^2}{\sqrt{1-\lambda^2}} \log \left(\frac{(1 + \sqrt{1-\lambda^2})(\lambda + \sqrt{1-c^2})}{\lambda(1 - c\sqrt{1-\lambda^2} + \lambda\sqrt{1-c^2})} \right)
\end{aligned}$$

We assume that both the total volume and area are conserved (due to balanced osmolarity and extremely high energy cost to stretch a bilayer), now the question becomes how to minimize the total energy expressed in three variables under both area ($A=A_0$) and volume constraints ($V=V_0$):

$$\begin{aligned}
E &= E_{bending} + E_{adhesion} \\
&= \frac{\kappa}{2} \oint (K_1 + K_2)^2 dA - W A^*
\end{aligned}$$

Here W is the adhesion strength per unit area while A^* is the area of the adhesion plane.

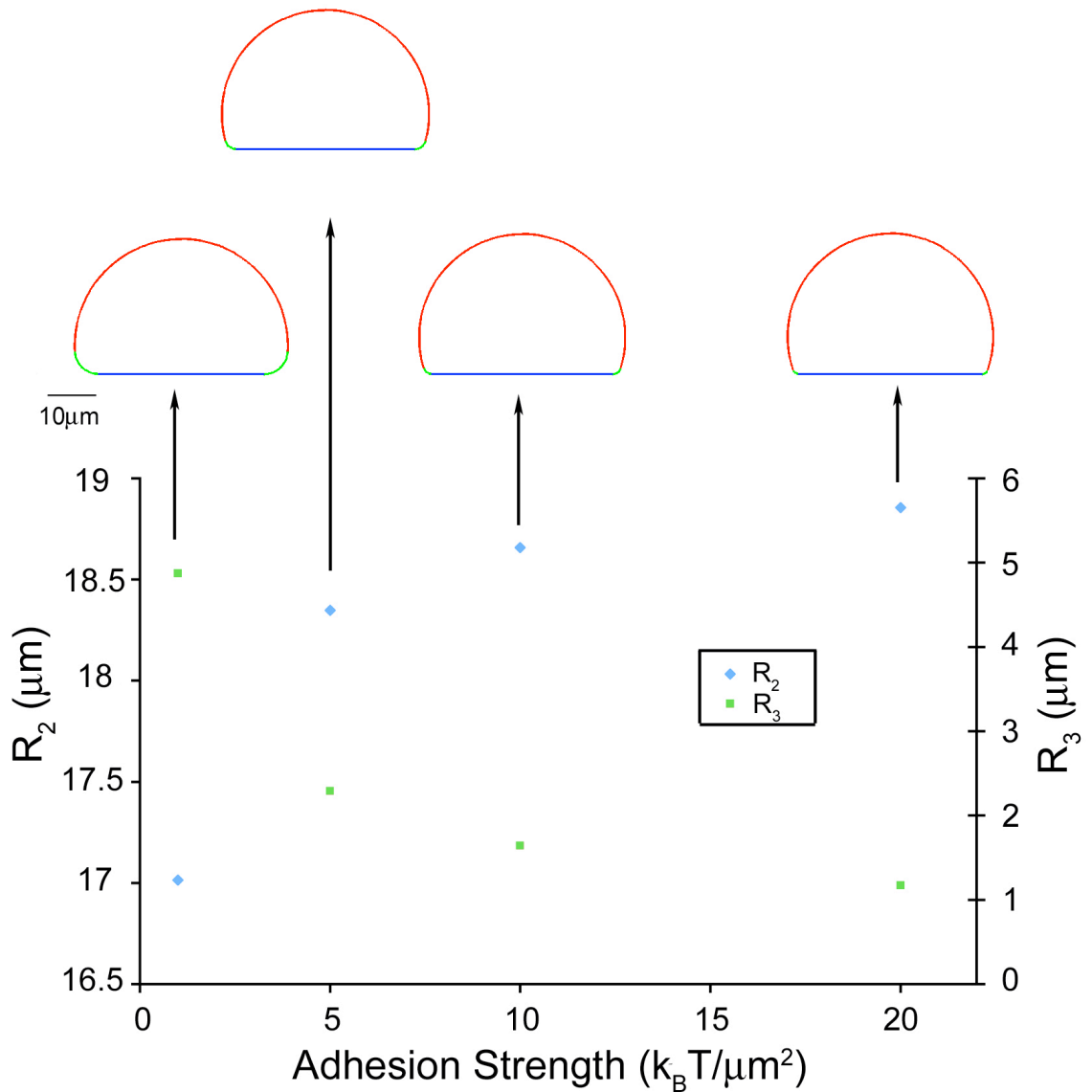


Figure 4. Representative simulation results based on energy minimization shows how the shape changes as adhesion strength increases. R_2 (blue, left axis) and R_3 (green, right axis) are plotted as functions of adhesion energy. The coloring scheme is the same in vesicle shape plots on the top of each set of data points (R_1 red, R_2 blue, and R_3 green). The initial state of the vesicle is represented by $R_0=20 \mu m$ and reduced volume $\sigma=0.9$ while the bilayer bending modulus is $\kappa=20 k_B T$ for DOPC bilayers (21).

Now that the model is complete, for any given adhesion strength W and initial volume and area, one can obtain a configuration (set of R_3 , λ , and c) that gives minimal total energy. Inverting the problem, one can start from a final configuration and deduce the adhesion strength W . The latter case is what really happens in the experiments – one can take confocal images of an adhering vesicle, reconstruct its three-dimensional configuration, and then calculate the corresponding adhesion strengths, which we are interested in. Before collecting experimental data, I did a few rounds of simulations to calculate the shapes of typical sized GUVs under different adhesion strengths (Figure 4). What the simulation results tell us is that under high adhesion strength, the shape change becomes minimal so that one cannot confidently resolve the differences (for example, see the green regions of vesicles at adhesion strengths 10 and 20 $k_B T/\mu\text{m}^2$). In this case, one can still obtain adhesion strength from experimental data but the confidence interval will be too big to be meaningful.

Deduction of adhesion strength from experimental data

With the model complete, we then proceeded to perform the adhesion experiments. Following the protocol in the Materials and Methods (see Figure 5A for the electroformation chamber), we generated GUVs with diameters ranging from a few microns to tens of microns (Figure 5B). After adding L1 protein and incubating for 30 minutes, the GUVs deformed significantly (Figure 5C and 5D). A strong rhodamine signal, created by two contacting membranes, was observed at the adhesion interface.

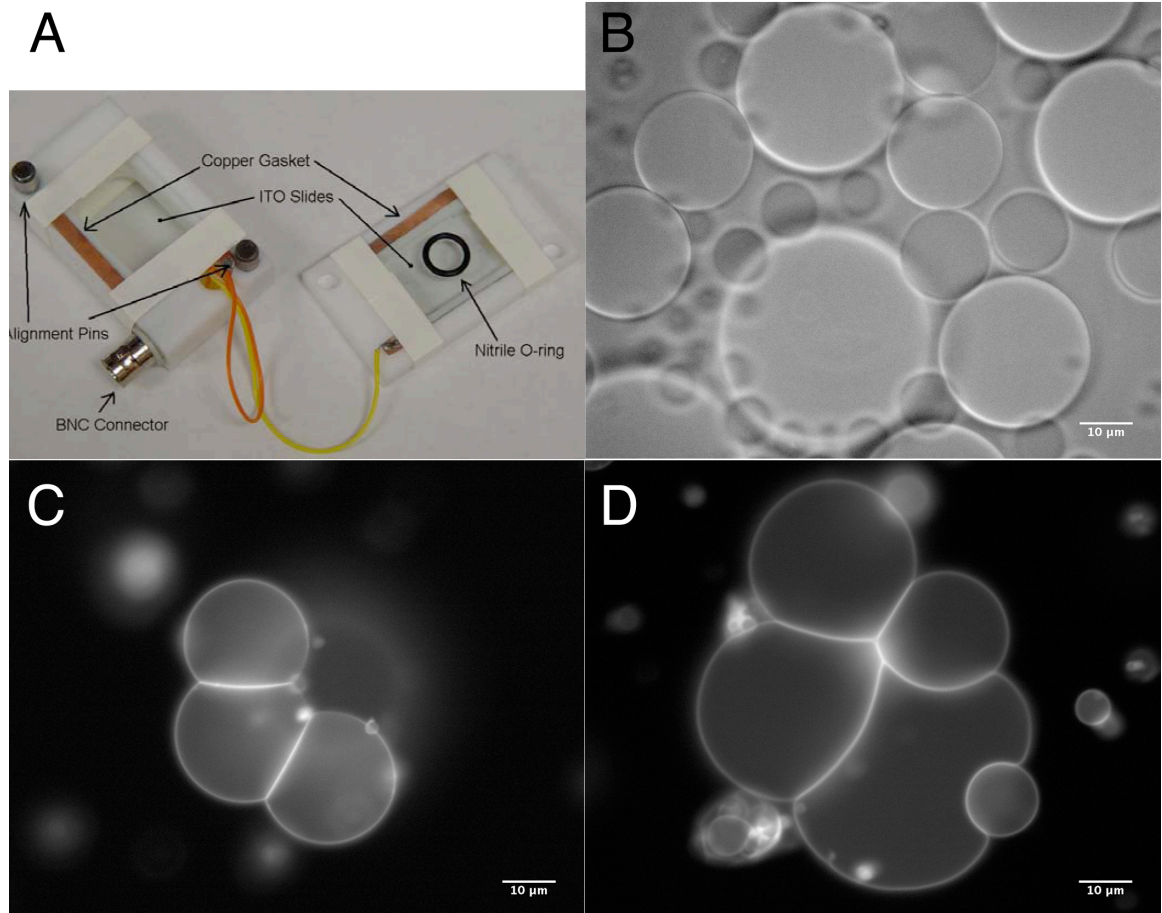


Figure 5. L1 adhesion induces significant deformations in adhering GUVs. (A) Electroformation chamber for GUV production (courtesy of Tristan Ursell). (B) DIC image of raw GUVs (before addition of L1) made from 5 mole % DOGS-NTA, 94.5% DOPC and 0.5% Rhodamine-PE. (C) and (D) fluorescent images of L1-mediated adhesion/deformation under rhodamine channel. All Scale bars are 10 μm.

Now that it was confirmed that adhesion could be observed on GUVs, we moved on to an experimental setup that mimics our model. As described in the Materials and Methods section, both GUVs and copper-NTA functionalized coverglass were incubated with L1 separately, and then the two were combined. We controlled the GUV density so that vesicle-vesicle adhesion was rarely observed and vesicle-coverglass adhesion was predominant. The sample was then imaged with a confocal microscope and stacks of images were taken on adhered GUVs along the z-axis, as described in the Materials and Methods section. The cross section of a typical adhered GUV is shown in Figure 6A; a negative control, in which no adhesion zone was observed, is shown in Figure 6B.

Data processing was carried out as described in the Materials and Methods section. At the end of this procedure, one set of parameters ($R_3 \lambda c$) is obtained using least square minimization to characterize the observed profile. Deriving adhesion energy from geometric parameters is simply the inverse problem of what was described in the previous simulation section. Calculated shape parameters and deduced adhesion energy densities from four different data sets are listed in Table 1 (see Figure 6C for fitting). These vesicles all had reduced volumes approaching unity, indicating that they were nearly spherical before adhesion occurred. This is consistent with the fact that the osmolarity difference between the inside and outside of vesicles was minimal because we used solutions of matching osmolarity to prepare and dilute the vesicles. The adhesion density varies greatly with vesicle size without an obvious trend. Obtaining more data may help reduce the confidence interval of the average adhesion energy density. It is also possible that adhesion energy does depend on the vesicle

size in a nontrivial way. One might think the redistribution of L1 molecule on GUV surface is able to cause the effect as long as the entropy cost can be compensated by adhesion. This hypothesis is based on the assumption that L1 protein is sparse enough on surface so that the adhesion zone needs more molecules to form. However, an analysis of the sizes of lipid molecule and L1 protein does not seem to support this theory. A lipid molecule normally occupies 0.25 nm^2 on surface (22) while a typical Ig domain or FNIII domain measures 3 nm in diameter and 5 nm along the long axis (data derived from crystal structures). This means that if the bilayer contains 5% DOGS-NTA as in our experiment, there are 5.7 DOGS-NTA molecules per the space one L1 molecule fills up. Since either the density of DOGS-NTA lipids or the steric effect of L1 itself determines the L1 density on GUV surface, it seems that there is no need for the adhesion zone to recruit L1 molecules from other regions of the GUV.

Table 1: Summary of information during data processing

	022409#2	022409#4	022409#5	022409#8
Data file	022409#2_stacks	022409#4_stacks	022409#5_stacks	022409#8_stacks
No. of images used	66	63	63	39
Centering images ¹	35-45	30-40	35-45	15-22
Data extraction threshold ²	1.3	1.3	1.8	1.5
No. of extracted data points	673	418	487	299
Index of best fit parameters	8	23	38	29
Error of best fit	0.0177	0.0153	0.0094	0.0116
Best fit parameters (R_3, λ, c)	(4.1860, 0.4654, 0.0503)	(3.1063, 0.4567, 0.0481)	(1.5555, 1.9417, -0.0413)	(1.6210, 0.8669, 0.0980)
Total area A_x	435	237	226	100
Reduced volume Σ_x	0.989	0.989	0.935	0.969
Center of spherical cap	(0, 4.09)	(0, 3.04)	(0, 1.68)	(0, 1.48)
Center of connecting region	(1.95, 4.19)	(1.42, 3.11)	(3.02, 1.56)	(1.41, 1.62)
Adhesion strength W^3	1.3	2.4	9.1	7.9
Min $f(x)$ during finding W	0.01423	0.01411	0.01915	0.00283

¹ Centering images were used to determine the axis of revolution.

² A pixel is considered to be a data point when its fluorescent value is greater than the mean value of fluorescence intensities for the current image plus the threshold times the standard deviation.

³ The unit of adhesion strength W is $k_B T / \mu\text{m}^2$. The bending modulus was taken as $20 k_B T$ when calculating the adhesion strength. The unit of length is μm unless specified otherwise.

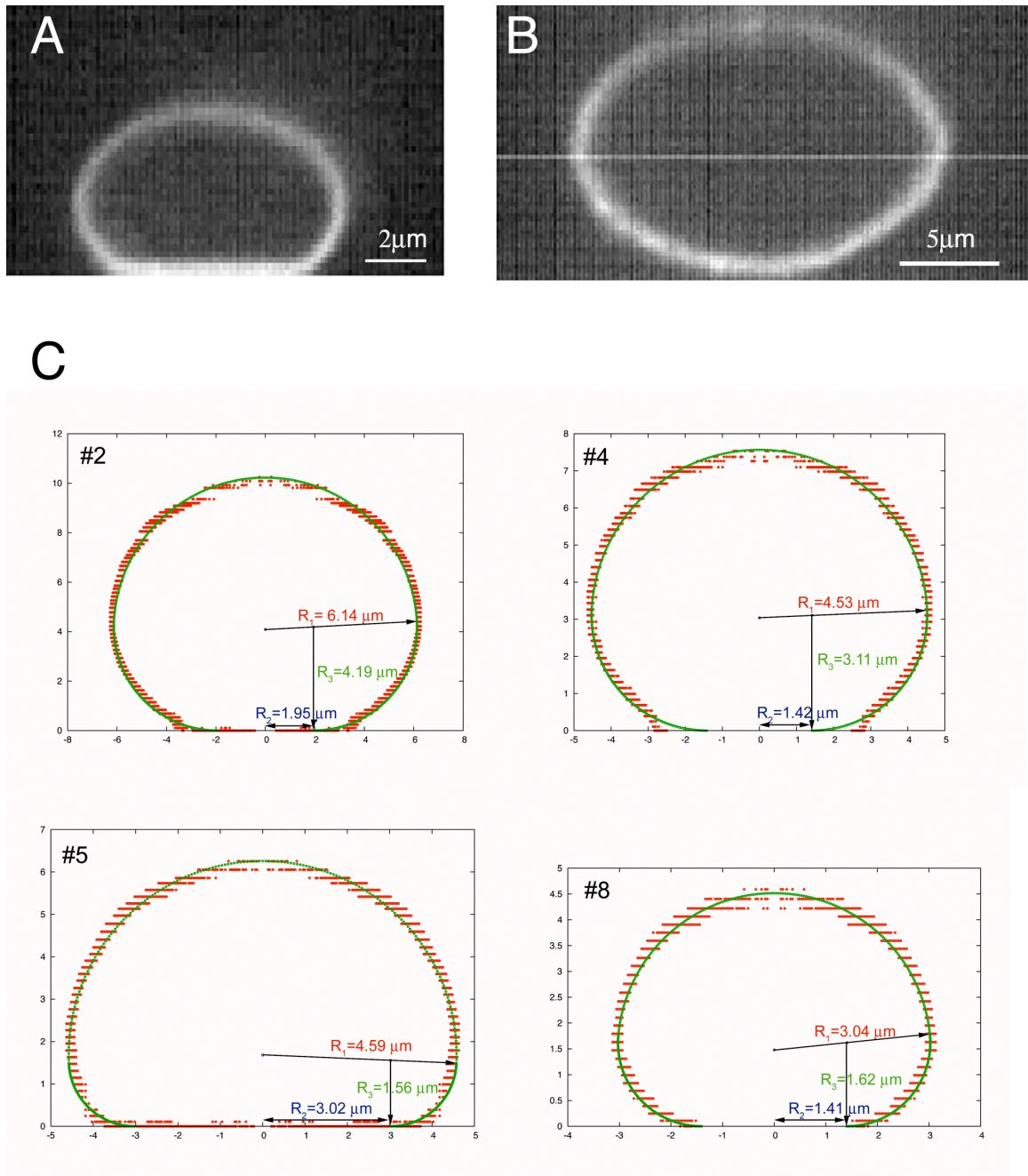


Figure 6. L1-mediated adhesion imaged by confocal microscopy. (A) Cross-section along yz plane of a GUV incubated with L1. (B) Cross section along yz plane of a GUV incubated with a control protein. Please note that z positions in A and B were not corrected with refractive index mismatch corrections. (C) Extracted confocal data (red) vs. fitting using our basis shape model (green) for all four data sets. The derived geometric parameters are shown in each panel and in Table 1.

Finally, the validity of the parameterized model should be verified to ensure the model was sufficient to describe the system under our experimental conditions. The next section describes my work on the validation of the basis shape model by checking it against numerically simulated profiles using Surface Evolver.

Surface evolver as a verification tool for the basis shape model

Surface Evolver (<http://www.susqu.edu/brakke/evolver/>) is a widely-used interactive software to simulate the shape statics of an object under mechanical forces (23). The software finds the optimal shape of an object by minimizing the total energy of the system. Normally, a user provides an initial shape and specifies the functional forms of various energies, and Surface Evolver then evolves the object shape along the gradient the energy hypersurface. The typical process of evolution is shown in Figure 7 and one can see how a cube becomes an adhered vesicle under the force determined by the gradient of the energy functional. Researchers have successfully applied this methodology in studying the formation of multicellular aggregates (24).

Surface Evolver simulation was carried out for different reduced adhesion strengths ($\gamma = WR_0^2/2\kappa$, in which W is the adhesion strength, R_0 is the characteristic length, and κ is the bending modulus). The numerical profile of deformed vesicles at $\gamma=1, 2, 5, 10$ were fitted to the basis shape model to evaluate its applicability. The comparison between the numerical result and the best fit model is shown in Figure 8. Qualitatively, vesicles under stronger adhesion ($\gamma=5$ and $\gamma=10$) seemed to be approximated better by the basis shape model. It should be noted that the numerical simulations are not always stable, especially for large adhesion strengths.

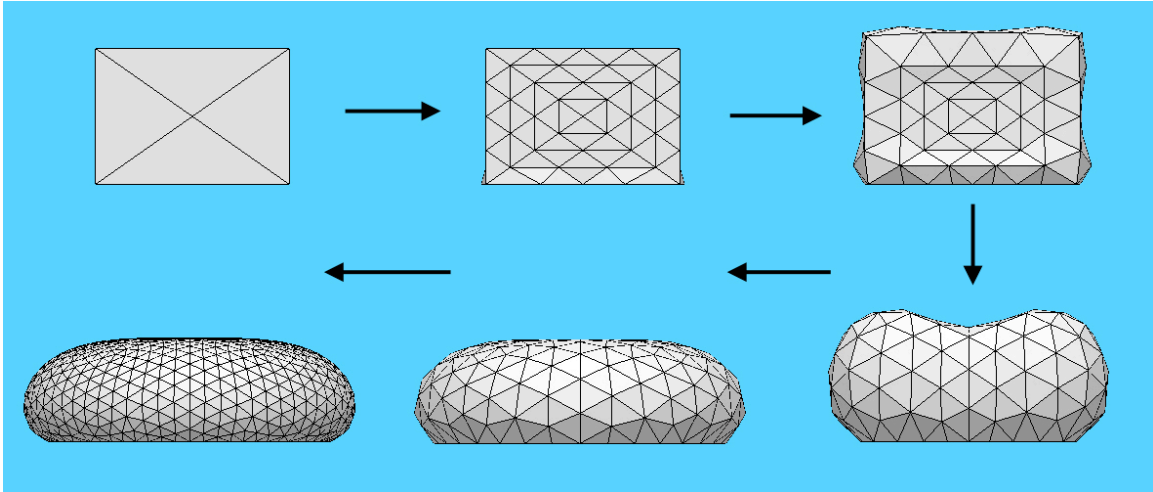


Figure 7. Typical evolution of a vesicle adhered to a flat substrate (total area $A=6$, total volume $V=1$, reduced volume $\sigma=V/[4\pi/3](A/4\pi)^{3/2}=0.72$).

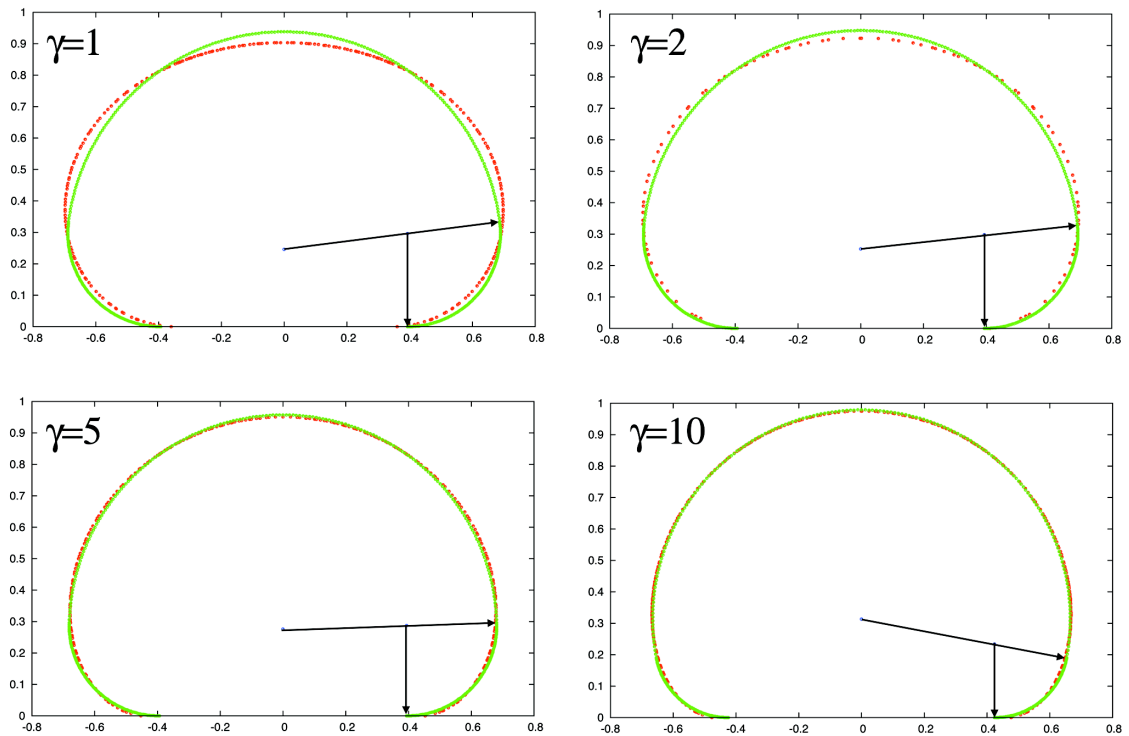


Figure 8. Comparison of numerical results by Surface Evolver (red) and best fitting using basis shape model. In all cases the reduced volume is 0.95, which is comparable with that in our experiment.

Future Directions

L1-GFP enables the direct visualization of L1 on GUVs

We described our observation of GUVs adhering to flat surface by monitoring the rhodamine signal within the lipid bilayer. However, this method does not give any information on the distribution of L1 protein on GUV surface and thus would not allow assessment of potential L1 relocalization once adhesion zone is initiated, one of the questions we aim to answer. In order to visualize the L1 protein, we designed a construct that has a GFP fused to the C-terminus of the L1 ectodomain. This protein, L1-GFP, was successfully expressed in mammalian cells and purified following the protocol used previously for L1 and its fluorescent signal was confirmed (Figure 9A). L1-GFP has also been proven to mediate adhesion between GUVs (Figure 9B). Therefore, we have now a tool to visualize the bilayer and the localization of L1 protein within the bilayer. We also tested the attachment of L1-GFP on copper-NTA functionalized coverglass and observed a fluorescent signal. After photobleaching, this signal did not recover (data not shown), indicating that this signal indeed came from immobilized L1-GFP, rather than residual protein in the aqueous phase.

Manipulation of lipid composition has proven to be feasible

Currently we use a lipid mixture containing 5% DOGS-NTA, which determines the maximum number of His-tagged L1 proteins the GUV can possibly attach. One possible assay is to monitor the GUV shape profiles while changing the percentage of DOGS-NTA lipids. We successfully made GUVs with 10% and 20% DOGS-NTA (Figure 10). However, lipid mixtures containing 50% DOGS-NTA failed to generate any GUVs.

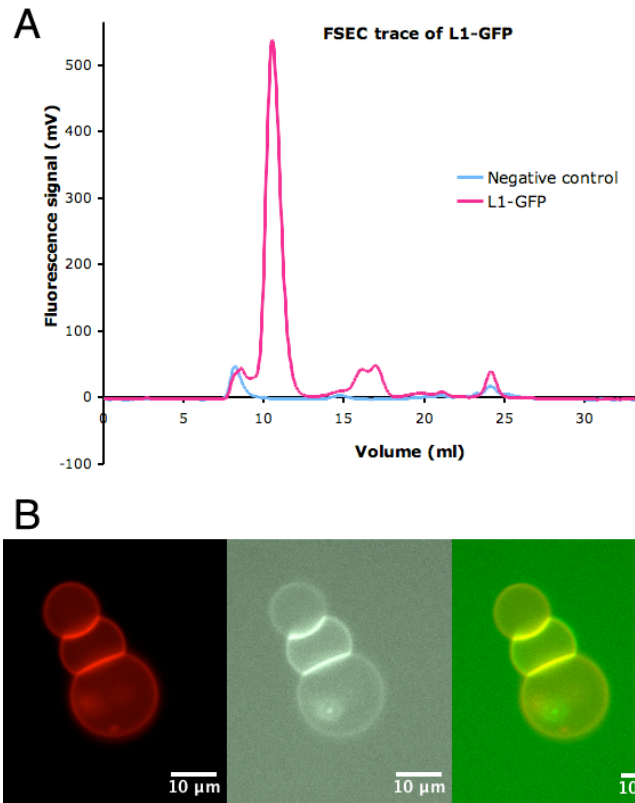


Figure 9. Recombinant L1-GFP is fluorescent and is able to induce vesicle deformation during adhesion. (A) Fluorescence size exclusion chromatography (FSEC) trace of purified L1-GFP. (B) GUV adhesion imaged under both rhodamine (left) and GFP (middle) channels, and the overlay of the two (right).

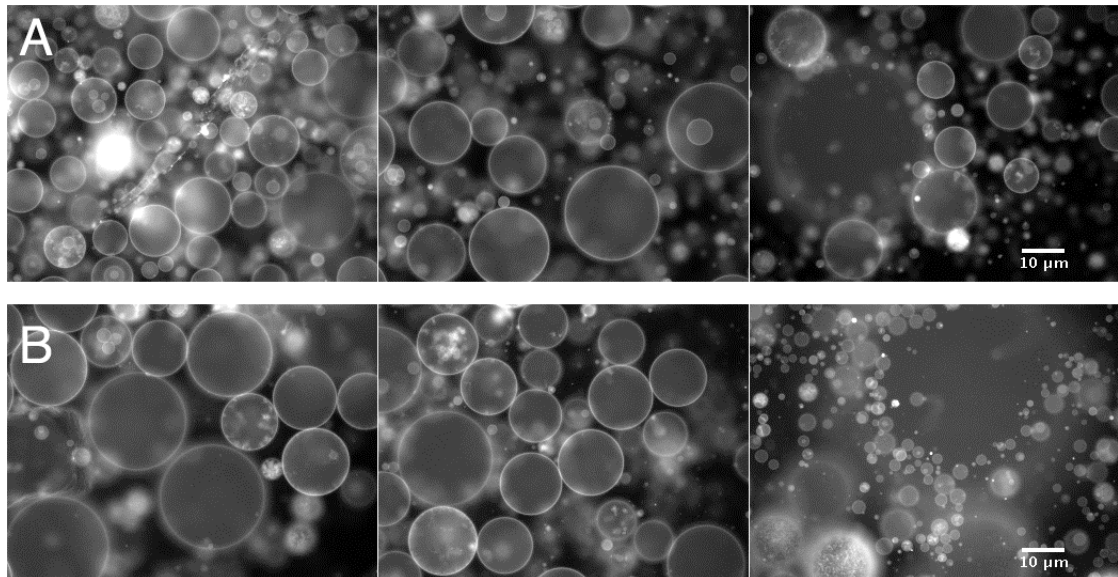


Figure 10. Successful production of GUVs from different lipid composition. (A) GUVs made from 10% DOGS-NTA. (B) GUVs made from 20% DOGS-NTA.

References:

1. Maness, P. F., and Schachner, M. (2007) Neural recognition molecules of the immunoglobulin superfamily: signaling transducers of axon guidance and neuronal migration, *Nat Neurosci* 10, 19-26.
2. Moos, M., Tacke, R., Scherer, H., Teplow, D., Fruh, K., and Schachner, M. (1988) Neural adhesion molecule L1 as a member of the immunoglobulin superfamily with binding domains similar to fibronectin, *Nature* 334, 701-703.
3. Brummendorf, T., Kenwrick, S., and Rathjen, F. G. (1998) Neural cell recognition molecule L1: from cell biology to human hereditary brain malformations, *Curr Opin Neurobiol* 8, 87-97.
4. Huang, Z. J. (2006) Subcellular organization of GABAergic synapses: role of ankyrins and L1 cell adhesion molecules, *Nat Neurosci* 9, 163-166.
5. Cohen, N. R., Taylor, J. S., Scott, L. B., Guillery, R. W., Soriano, P., and Furley, A. J. (1998) Errors in corticospinal axon guidance in mice lacking the neural cell adhesion molecule L1, *Curr Biol* 8, 26-33.
6. Kenwrick, S., Watkins, A., and De Angelis, E. (2000) Neural cell recognition molecule L1: relating biological complexity to human disease mutations, *Hum Mol Genet* 9, 879-886.
7. Irintchev, A., Koch, M., Needham, L. K., Maness, P., and Schachner, M. (2004) Impairment of sensorimotor gating in mice deficient in the cell adhesion molecule L1 or its close homologue, CHL1, *Brain Res* 1029, 131-134.

8. Wiencken-Barger, A. E., Mavity-Hudson, J., Bartsch, U., Schachner, M., and Casagrande, V. A. (2004) The role of L1 in axon pathfinding and fasciculation, *Cereb Cortex 14*, 121-131.
9. Su, X. D., Gastinel, L. N., Vaughn, D. E., Faye, I., Poon, P., and Bjorkman, P. J. (1998) Crystal structure of hemolin: a horseshoe shape with implications for homophilic adhesion, *Science 281*, 991-995.
10. Schurmann, G., Haspel, J., Grumet, M., and Erickson, H. P. (2001) Cell adhesion molecule L1 in folded (horseshoe) and extended conformations, *Mol Biol Cell 12*, 1765-1773.
11. Freigang, J., Proba, K., Leder, L., Diederichs, K., Sonderegger, P., and Welte, W. (2000) The crystal structure of the ligand binding module of axonin-1/TAG-1 suggests a zipper mechanism for neural cell adhesion, *Cell 101*, 425-433.
12. He, Y., Jensen, G. J., and Bjorkman, P. J. (2009) Cryo-electron tomography of homophilic adhesion mediated by the neural cell adhesion molecule L1, *Structure 17*, 460-471.
13. Seifert, U. (1997) Configurations of fluid membranes and vesicles, *Advances in Physics 46*, 13-137.
14. Svetina, S., and Zeks, B. (1989) Membrane Bending Energy and Shape Determination of Phospholipid-Vesicles and Red Blood-Cells, *European Biophysics Journal with Biophysics Letters 17*, 101-111.
15. Miao, L., Seifert, U., Wortis, M., and Dobereiner, H. G. (1994) Budding Transitions of Fluid-Bilayer Vesicles - the Effect of Area-Difference Elasticity, *Physical Review E 49*, 5389-5407.

16. Seifert, U., and Lipowsky, R. (1990) Adhesion of Vesicles, *Physical Review A* 42, 4768-4771.
17. Seifert, U. (1991) Adhesion of Vesicles in 2 Dimensions, *Physical Review A* 43, 6803-6814.
18. (1999) CRC handbook of chemistry and physics, Chapman and Hall/CRCnetBASE, Boca Raton, FL.
19. Huang, B., Jones, S. A., Brandenburg, B., and Zhuang, X. (2008) Whole-cell 3D STORM reveals interactions between cellular structures with nanometer-scale resolution, *Nat Methods* 5, 1047-1052.
20. Egner, A., and Hell, S. W. (1999) Equivalence of the Huygens-Fresnel and Debye approach for the calculation of high aperture point-spread functions in the presence of refractive index mismatch, *Journal of Microscopy-Oxford* 193, 244-249.
21. Fa, N., Lins, L., Courtoy, P. J., Dufrene, Y., Van Der Smissen, P., Brasseur, R., Tyteca, D., and Mingeot-Leclercq, M. P. (2007) Decrease of elastic moduli of DOPC bilayers induced by a macrolide antibiotic, azithromycin, *Biochim Biophys Acta* 1768, 1830-1838.
22. Phillips, R., Kondev, J., and Theriot, J. (2009) *Physical biology of the cell*, Garland Science, New York.
23. Brakke, K. A. (1996) The surface evolver and the stability of liquid surfaces, *Philosophical Transactions of the Royal Society of London Series a-Mathematical Physical and Engineering Sciences* 354, 2143-2157.

24. Zihlerl, P., and Svetina, S. (2007) Flat and sigmoidally curved contact zones in vesicle-vesicle adhesion, *Proceedings of the National Academy of Sciences of the United States of America* 104, 761-765.